

# Topological phase transitions in two-dimensional bent-core liquid crystal models

B. Kamala Latha<sup>1,\*</sup>, Surajit Dhara<sup>1</sup>, and V. S. S. Sastry<sup>2</sup>

<sup>1</sup>*School of Physics, University of Hyderabad, Hyderabad 500046, India*

<sup>2</sup>*Centre for Modelling, Simulation and Design, University of Hyderabad, Hyderabad 500046, India*



(Received 30 June 2021; accepted 23 November 2021; published 13 December 2021)

Two-dimensional liquid crystal (LC) models of interacting V-shaped bent-core molecules with two rigid rodlike identical segments connected at a fixed angle ( $\theta = 112^\circ$ ) are investigated. The model assigns equal biquadratic tensor coupling among constituents of the interacting neighboring molecules on a square lattice, allowing for reorientations in three dimensions ( $d = 2$ ,  $n = 3$ ). We find evidence of two temperature-driven topological transitions mediated by point disclinations associated with the three ordering directors, condensing the LC medium successively into uniaxial and biaxial phases. With Monte Carlo simulations, temperature dependencies of the system energy, specific heat, orientational order parameters, topological order parameters, and densities of unbound topological defects of the different ordering directors are computed. The high-temperature transition results in topological ordering of disclinations of the primary director, imparting uniaxial symmetry to the phase. The low-temperature transition precipitates simultaneous topological ordering of defects of the remaining directors, resulting in biaxial symmetry. The correlation functions, quantifying spatial variations of the orientational correlations of the molecular axes show exponential decays in the high-temperature (disordered) phase, and power-law decays in the low-temperature (biaxial) phase. Differing temperature dependencies of the topological parameters point to a significant degree of cross coupling among the uniaxial and biaxial tensors of interacting molecules. This simplified Hamiltonian leaves  $\theta$  as the only free model parameter, and the system traces a  $\theta$ -dependent trajectory in a plane of the phenomenological parameter space.

DOI: [10.1103/PhysRevE.104.064701](https://doi.org/10.1103/PhysRevE.104.064701)

## I. INTRODUCTION

The self-organizing property of soft matter leads to myriad applications in the fields of optics, biosensors, and electronics. The formation of liquid crystal (LC) phases on two-dimensional (2D) surfaces is the key to many nanotechnological applications [1,2]. It is established that continuous symmetries cannot be spontaneously broken at finite temperature in systems with sufficiently short-range interactions in dimensions  $d \leq 2$  [3]. However, low-temperature phases with quasi-long-range order (QLRO) are still realizable in such systems in the presence of stable topological defects, made permissible through a choice of nontrivial topology of the corresponding order parameter (OP) space ( $\mathcal{R}$ )—a phenomenon detected in the 2D-XY ( $d = 2$ ) magnetic model through the Berezinskii-Kosterlitz-Thouless (BKT) mechanism [4,5]. LCs with global  $SO(3)$  symmetry and a local site symmetry of  $Z_2$  (uniaxial systems) have  $\mathcal{R}$  which is not simply connected. This OP geometry leads to the presence of point defects in 2D uniaxial as well as biaxial nematics. The fundamental group of  $\mathcal{R}$  for uniaxial nematics (with  $D_{\infty h}$  point-group symmetry) is isomorphic to the two-element Abelian group  $\Pi_1(\mathcal{R}) = Z_2$ . In two dimensions, this provides for stable point disclinations with topological charge (winding number) with a value  $\pm 1/2$ , corresponding to rotation of the order director by  $180^\circ$  (in  $\mathcal{R}$ ) for a closed path in the physical space. For

biaxial nematics which have a global point group symmetry  $D_2$ , the OP space is  $\mathcal{R} = SO(3)/D_2$ . Taking the homomorphic correspondence between  $SO(3)$  and  $SU(2)$ , this becomes  $\mathcal{R} = SU(2)/Q$  where  $Q$  is the lift of  $D_2$  in  $SU(2)$ . Thus the fundamental group of biaxial nematics is  $\Pi_1(\mathcal{R}) = Q$ , the eight-element quaternion group which is discrete and non-Abelian. The eight elements can be grouped into five conjugacy classes  $C_0$ ,  $\bar{C}_0$ ,  $C_x$ ,  $C_y$ , and  $C_z$ . The class  $C_0 = [1]$  contains removable defects,  $\bar{C}_0 = [-1]$  contains  $360^\circ$  disclinations and classes  $C_x = [\pm i\sigma_x]$ ,  $C_y = [\pm i\sigma_y]$  and  $C_z = [\pm i\sigma_z]$  (where  $\sigma_x, \sigma_y, \sigma_z$  are Pauli matrices) contain defects in which the rotation is through  $\pm 180^\circ$  about each of the distinct symmetry axes. Thus stable defects of both integer and half-integer charges exist in biaxial nematics [3]. The above criterion for the condensation of QLRO phases applies readily to lattice models of LC systems, since the corresponding Hamiltonians engage only angular displacements of the interacting constituents, decoupled from translational degrees of freedom [6].

The BKT disclination unbinding scenario in the ( $n = 2$ ,  $d = 2$ ) uniaxial lattice model (Lebwohl-Lasher interaction [7]), wherein the reorientations of molecules on the 2D-lattice sites ( $d = 2$ ) are restricted to a plane ( $n = 2$ ), is formally equivalent to the 2D-XY model, as verified through simulations. This model exhibits a low-temperature nematic phase (of uniaxial symmetry) with a QLRO phase. Similar observations were made earlier on other ( $d = 2$ ,  $n = 2$ ) models, like ensembles of hard rods [8,9], spherocylinders [10], and hard bent needles [11]. These studies indicated evidence of

\*Corresponding author: [kkkata@gmail.com](mailto:kkkata@gmail.com)

disclination unbinding, leading to transitions from isotropic to quasinematic phase.

In this paper, we investigate the phase behavior of a system of LC molecules with a bent-core geometry (V shape) located on a square lattice, and enjoying a three-dimensional degree of freedom for reorientations ( $d = 2$ ,  $n = 3$ ). This paper is motivated by a recent investigation of a general biquadratic Hamiltonian [12–14] with a  $D_{2h}$  site symmetry ( $d = 2$ ,  $n = 3$ ) with certain simplifying conditions [15]. Therein it was assumed that the biaxial model has minimal coupling interactions, with no cross interaction among uniaxial tensors of an interacting site with biaxial tensors of its neighbors. Further, the biaxial model parameter is tuned to result in a strong and direct (thermally driven) transition from disordered to the biaxial phase. A detailed Monte Carlo (MC) study demonstrated a topological transition to a low-temperature phase with  $D_{2h}$  global symmetry, characterized by the continual presence of equilibrium states with self-similar structures (power-law behavior of spatial correlations of molecular orientations), with variation of temperature (often described as a phase exhibiting a line of critical points over the relevant temperature region). These observations are supported by the computed topological variables and their low-temperature limits. This work in Ref. [15], besides confirming a BKT-type topological transition in a 2D biaxial phenomenological model, also provided independent evidence supporting the conjecture made to explain the observed crossover in the 2D-LL system [16]. The requirement to add a suitable biaxial perturbation to the 2D uniaxial model to avoid the crossover reported, explicitly pointed to the prerequisite condition to reduce the topological symmetry of  $\mathcal{R}$  so as to make its fundamental group discrete and non-Abelian, making it a necessary criterion for this interesting defect-mediated transition. In the current paper, we examine this conjecture further by choosing a biaxial lattice model (with bent-core molecules) with a local site symmetry different from the known global symmetry of the low-temperature (biaxial) phase. The model is based on a microscopic molecular-level prescription of interactions, which facilitates explicit choices regarding the molecular geometry and the degree of different interactions.

To develop an appreciation of the chosen bent-core model within the context of the well-established phenomenological models, and with the objective of making a correspondence with their parameters, it is useful to briefly introduce the general biquadratic Hamiltonian for biaxial systems accounting for the interactions among the molecular tensors with uniaxial and biaxial symmetry, along with the phenomenological model parameters. Its phase diagram in three dimensions was extensively investigated earlier [12–14,17], specifically providing insights into the role of the two types of biaxial coupling hosted in the Hamiltonian. The recent 2D-biaxial study mentioned above [15] is a particularly simplifying choice of these parameters.

The interaction between two lattice sites, each possessing in general a biaxial symmetry, is expressed in terms of the two orthogonal and traceless molecular tensors associated with each site:  $\mathbf{q} := \mathbf{m} \otimes \mathbf{m} - \frac{I}{3}$  (uniaxial symmetry) and  $\mathbf{b} := \mathbf{e} \otimes \mathbf{e} - \mathbf{e}_\perp \otimes \mathbf{e}_\perp$  (biaxial symmetry). Here  $(\mathbf{e}, \mathbf{e}_\perp, \mathbf{m})$  is an orthonormal set of vectors representing the molecular

axes (in the notation of Ref. [12]). The system Hamiltonian, inclusive of the biaxial symmetry, is expressed in terms of a general interaction between two lattice sites  $(i, j) : H_{ij} = -U[\xi \mathbf{q}_i \cdot \mathbf{q}_j + \gamma(\mathbf{q}_i \cdot \mathbf{b}_j + \mathbf{q}_j \cdot \mathbf{b}_i) + \lambda \mathbf{b}_i \cdot \mathbf{b}_j]$ . The Lebwohl-Lasher (LL) model corresponds to limiting this expression to uniaxial symmetry by setting  $\xi = 1$ ,  $\gamma = 0$ ,  $\lambda = 0$ . The 2D-LL model (with  $d = 2$ ,  $n = 3$ ) was extensively studied both with Metropolis algorithm [18,19] and recently with entropic sampling method [16]. The phenomenological 2D biaxial model referred to earlier [15] corresponds to setting  $\xi = 1$ ,  $\gamma = 0$ ,  $\lambda = 1/3$ . It is expected that the bent-core model could be a promising candidate to provide insight into the phase behavior of a general model with contributions from all three terms. In this context, the bent-core model in its general form [20] facilitates effective variation of the parameters  $\gamma$  and  $\lambda$  in the phenomenological model.

The paper is organized as follows. In Sec. II, we present the Hamiltonian model and the simulation details. The data are presented and results of their detailed analysis are discussed in Sec. III. We conclude with a summary of the salient features of this work in Sec. IV.

## II. MODEL AND SIMULATION DETAILS

### A. Model and Hamiltonian

We investigated the 2D phase behavior of a simplified V-shaped bent-core system with identical rodlike arms bent at angle  $\theta = 112^\circ$  and with equal inter-arm coupling strengths. To assign an orthonormal triad fixed to the molecule, the symmetry axes of the molecule  $(x, y, z)$  are chosen as (i)  $x$  axis corresponds to the direction orthogonal to the molecular plane at the vertex, (ii)  $y$  axis is the direction bisecting the angle between the two arms of the molecule, and  $z$  axis is mutually perpendicular to these two directions, completing a right-handed triad. When the arms are orthogonal to each other ( $\theta = 90^\circ$ ), the interaction tensor for these molecules is cylindrically symmetric about the  $x$  axis (perpendicular to the arms). The molecule is disklike for angles  $90^\circ < \theta < 109.47^\circ$  and rodlike for angles  $109.47^\circ < \theta < 180^\circ$ ;  $\theta = 109.47^\circ$  (i.e.,  $\cos(\theta) = -1/3$ ) being the angle of tetrahedral geometry for the molecule. As the interarm angle increases from  $90^\circ$  to  $180^\circ$ , the molecular interaction tensor acquires contributions from both uniaxial and biaxial tensorial components, the relative importance of which impacts the formation of the respective phases. The simulation studies of phase behavior of these molecules in three dimensions ( $d = 3$ ) interacting through an attractive biquadratic potential revealed an isotropic (I)-uniaxial nematic ( $N_U$ )-biaxial nematic ( $N_B$ ) phase sequence for various interarm angles and different interaction strengths between the arms. A direct isotropic to biaxial transition is also predicted for the interarm angle of  $\theta = 109.47^\circ$ , for unit interaction strength [20]. In this paper, we chose the  $\theta$  value so as to lead to a prolate uniaxial phase on condensation from the isotropic phase by the orientational ordering of the major molecular axes associated with the primary director ( $z$  axes). On further condensation, a biaxial phase forms induced by the ordering of the two minor molecular axes ( $x$  and  $y$  axes). The nontrivial topological

symmetry of  $\mathcal{R}$  of this system results in its fundamental group  $\Pi_1(R) = Q$ , and hence to the existence of stable topological defects with differing charges (winding numbers) in the medium. We expect, from earlier 2D work, this model to host thermally induced topological transitions, with an underlying BKT-type unbinding mechanism primarily involving half-charge disclinations associated with the three director axes. The topologically ordered phases that the system may form depending on the chosen model parameters, are evidenced by their corresponding characteristic microscopic structures with QLRO and by sharp variations of the respective topological variables which quantify the degree of binding of the point defects.

The V-shaped LC system is modeled as a simple extension of the uniaxial LL lattice model [20]. Here, a lattice site hosts a mesogenic molecule made up of two rodlike constituents A and B joined at a fixed angle  $\theta$ . These two constituents interact with those of the four nearest-neighboring molecules on the square lattice. The interaction potential between two neighbors (with identical constituents) at two such lattice sites  $i$  and  $j$  is expressed as

$$U(\omega_{ij}) = - \sum_{\alpha=A,B} \sum_{\beta=A,B} \epsilon_{\alpha\beta} P_2(\cos(\gamma_{\alpha\beta})), \quad (1)$$

where the indices  $\alpha$  and  $\beta$  run over the two constituent segments of each molecule on the sites at  $i$  and  $j$ , respectively. Here  $\gamma_{\alpha\beta}$  is the angle between the arm  $\alpha$  of molecule at site  $i$  and arm  $\beta$  of molecule at  $j$ . For symmetric molecules, the degree of anisotropy of interaction is the same among all arms and is given by  $\epsilon_{AA} = \epsilon_{AB} = \epsilon_{BB} = \epsilon_{BA} = \epsilon$ . The system energy is expressed in units of  $\epsilon$ , and the reduced temperature for simulation purposes is specified as  $T = \frac{K_B T'}{\epsilon}$ , where  $T'$  is the laboratory temperature (in Kelvin).

### B. Simulation details

Simulations were carried out using both the Metropolis-based MC sampling and entropic sampling methods. The Metropolis algorithm [21] (Markov chain MC sampling) facilitates an otherwise perfectly random walk of the system in the (ergodic) configuration space, but for making the criterion of the acceptance, or otherwise, of each such random step respect the Boltzmann equilibration condition at the chosen temperature  $T$ . The underlying algorithm ensures that the system, starting from an arbitrary initial state, converges to a sequence of equilibrated microstates in the asymptotic limit of a long enough walk. A large enough set of equilibrated states follows the canonical distribution at  $T$ , constituting the Boltzmann ensemble (B ensemble). The averages of relevant physical observables are computed as averages over these microstates.

Entropic sampling, on the other hand, is geared to make the system representatively visit regions of the configuration space, with a distribution which is reasonably uniform with respect to the system energy (entropic sampling). The Wang-Landau (WL) algorithm [22] is an efficient procedure to achieve this objective, in the process estimating representative density of states (DoS) of the system  $g(E)$  (with respect to energy). This algorithm is now generalized to be applicable in different areas of research, like finite den-

sity quantum field theories [23], complex magnetic systems [24], polymers and protein folding [25], and spin crossover systems [26] and is being continually updated with parallel processing algorithms on multiple nodes using, for example, replica exchange protocol [27]. The original WL algorithm [22] was modified for different model systems, for example, for lattice systems with LL interaction potential [7], which requires continuous molecular reorientations in LC models [28]. It was further augmented by the so-called frontier sampling technique [29,30]. The latter is an interesting algorithm to force the system to visit progressively lower energy states (with extremely low probability), by setting up energy barriers at chosen points on the energy axis (referred to as frontiers), thereby discouraging temporarily access to higher energy regions (where the DoS has been already estimated approximately) until the system samples the lower energy states in the neighborhood of the barrier sufficiently. This process is continued till the desired energy range is covered. The underlying guiding distribution function generated by continuous upgrades during this walk provides an approximate estimate of  $g(E)$ . At this stage, the random walk is allowed to proceed according to the normal WL algorithm with no more energy barriers. The updating of the distribution function is continued while gradually reducing the algorithmic guidance, till  $g(E)$  is determined to the desired accuracy, normally limited by the cumulative computational errors. This limit of  $g(E)$  is considered as the representative DoS of the system. A large entropic ensemble of microstates ( $\sim 10^8$ ) is then collected by performing a random walk in the configuration space with an acceptance probability based on the inverse of  $g(E)$ . The ensemble of states so collected for a well-converged  $g(E)$  is reasonably uniformly distributed with energy typically to within 15-20% (despite humongous change in the entropy over the energy). The relevant equilibrium averages of observables are computed at the desired temperature by extracting equilibrium ensembles from the set of states in the entropic ensemble by the standard reweighting procedures [31,32] (RW ensembles). Further details of this modified WL algorithm augmented by frontier sampling can be found in Refs. [17,30].

Besides the richness of the configuration space in terms of accessible states in such LC models due to the continuous nature of the random steps of the system, another factor which significantly puts a huge demand on the computational time is the shape of the molecule, as well as the prescription set by the Hamiltonian. In the present model, the computational effort is considerably enhanced due to the fact that the directions of the interacting constituents of the mesogenic unit at the lattice site do not coincide with the orthonormal triad representing the orientation of the molecule, the latter being a necessity to effect tractable reorientations. This requires an intermediate Euler transformation to be performed during the calculation of energy, every time a reorientational random step is taken by the molecule, resulting in a significant increase in the computational effort. For example, the typical time for estimating the DoS of this system with size  $60 \times 60$  is of the order of 10–12 weeks on a single processor (as a serial job), which is about an order of magnitude more than what is required for a similar computation, but without the intermediate transformations.

We attempted to reduce the computing time by adopting a parallel computation of the DoS in different subsegments of the total energy range, based on the concept suggested in the replica-exchange MC algorithm [27]. Accordingly, the energy range of interest is divided into  $k$  equal, and significantly overlapping, segments. The DoS in each segment is determined to the required accuracy employing the above procedure through separate computations simultaneously on  $k$  processors. These components of the DoS corresponding to the different energy segments, computed on a logarithmic scale, differ from each other by an arbitrary constant, which is specific to each of the overlap regions. This allows for synthesizing the total DoS over the entire region by stitching them suitably, which can then be used for constructing entropic ensemble of the system over the total energy range, as outlined above. Alternatively, one can also determine the equilibrium properties of the system corresponding to each energy segment from its independently generated entropic (sub)ensemble, and finally obtain their variation over the total temperature range by a similar stitching process for each observable. We find the latter procedure to be more practical for our current application. Determination of the DoS over the total energy range is, however, necessary if a study of the free-energy profiles in the space of relevant observables is desired. For large system sizes, entropic sampling-based simulations were performed with this parallelization scheme, choosing  $k=4$ , and an overlap of 70% between contiguous energy segments. With this choice, we have large regions of overlap making the stitching process seamless and reliable, and we observed nearly 40% reduction in the computing time. We compared this composite data obtained through segmental computations with a single energy-window result for consistency, and the results matched extremely well.

It is known from earlier MC simulations on 2D-LC systems that conventional Metropolis-based sampling procedures may sometimes lead to qualitatively different conclusions, relative to those derived from data based on reweighted ensembles (entropic sampling procedure). In the 2D-LL model, the two methods resulted in qualitatively different outcomes: averages of observables from the B ensembles indicated convincing evidence for a transition to a topologically ordered low-temperature state, while the entropic sampling-based RW ensembles pointed to an intervening crossover denying topological ordering of the low-temperature phase [16]. On the other hand, in a biaxial system exhibiting a direct transition from the isotropic to biaxial phase (simultaneously engaging all the spin degrees in the mediation of the transition), both these sampling procedures led to identical results (within computational errors) [15]. It is thus not *a priori* clear which sampling procedure is sufficient, or necessary, to obtain reliable inferences on a system with well-separated uniaxial and biaxial transitions, and its phenomenological model is possibly rich with all three interaction terms. Thus we need to construct both B and RW ensembles for this model for comparison, and evaluation of its utility. To have comparable sampling errors between these two procedures, the Metropolis averages are computed, after due equilibration, over a production run of  $10^6$  MC lattice sweeps. RW ensembles are obtained through reweighting procedure from an entropic ensemble of  $\sim 10^8$  microstates.

Simulations were carried out on square lattices of size  $L \times L$  ( $L = 40, 60, 80, 100$ ), embedded in, say the laboratory YZ plane, with periodic boundary conditions enforced in the two orthogonal directions. Each lattice site hosts a symmetric V-shaped molecule with a fixed interarm angle  $\theta = 112^\circ$  and the molecules at each lattice site interact through the nearest-neighbor interaction in Eq. (1). The observables derived from both types of ensembles were indistinguishable for sizes  $L = 40$  and 60 (within errors). Considering the fact that the computational cost of the entropic procedure does not scale linearly with the number of molecules in the sample—unlike the Metropolis method—we opted for the Metropolis procedure for the two higher sizes. We chose to present mixed data from both sampling processes in different figures on purpose to stress the equality of the two procedures in this model.

The computed physical observables of interest are the average energy  $\langle E \rangle$ , specific heat  $\langle C_v \rangle$ , the uniaxial ( $R_{00}^2$ ), and biaxial ( $R_{22}^2$ ) order parameter of the LC phase [30]. Further, we computed topological properties related to the dominant charge 1/2 defects associated with the three order directors. The topological densities  $d_k$  ( $k = x, y, z$ ) are measures of the abundance of the isolated unbound charge 1/2 defects in the lattice, associated with the respective directors. Their averages  $\langle d_k \rangle \propto \exp(-E_{0k}/T)$  at low temperatures, where  $\langle E_{0k} \rangle$  is the activation energy required to break a bound defect associated with the respective  $k$ th director to create a pair of oppositely charged defects [33]. Another quantity of interest is the topological order  $\mu$  which measures the degree of pairing of defects in a lattice configuration at that temperature, averaged over the production run.  $\mu$  takes values  $0 \leq \mu \leq 1$ , where  $\mu = 0$  denotes the presence of only free defects and  $\mu = 1$  denotes complete pairing. A related derived quantity  $\delta = (1 - \mu)/2$  is computed and takes values  $0 \leq \delta \leq 0.5$  [18]. We calculated the topological densities ( $d_x, d_y, d_z$ ) and the topological order parameter ( $\delta_x, \delta_y, \delta_z$ ) of the (X, Y, Z) directors, respectively, where the subscript denotes the defects associated with each of the ordering directors. These calculations are described in detail in Ref. [15]. The above data are computed as a function of temperature in the range [0.05, 1.5] with a resolution of 0.005. Spatial variations of orientational pair correlations (correlation functions)  $G(r_{ij}) = \langle P_2(\cos \varphi_{ij}) \rangle$ , are computed for the three molecular symmetry axes ( $x, y, z$ ) (at  $L = 100$ ), denoted as  $G_x(r)$ ,  $G_y(r)$ , and  $G_z(r)$ . The correlation functions are computed at 60 temperatures representatively covering this range. Statistical errors, estimated with the jack-knife algorithm [34], in  $E$ ,  $R_{00}^2$ ,  $R_{22}^2$ ,  $\delta_{x,y,z}$  and  $d_{x,y,z}$  are typically of the order of 1 in  $10^3$ , while higher moments ( $C_v$ ) and Binder's energy cumulant  $E_4$  [35] are relatively less accurate (about 5 in  $10^2$ ).

### III. RESULTS AND DISCUSSION

We present data for different sizes choosing WL-ensemble-based results at  $L = 40$  and 60, and B-ensemble results at  $L = 80$  and 100 to explicitly indicate the equivalence of the two sampling procedures for the model at this  $\theta$ . Figure 1 depicts the temperature variation of  $C_v$  (per site) for system sizes  $L = 40, 60, 80, 100$ . As the temperature is lowered from the isotropic phase (at a given system size), the specific heat



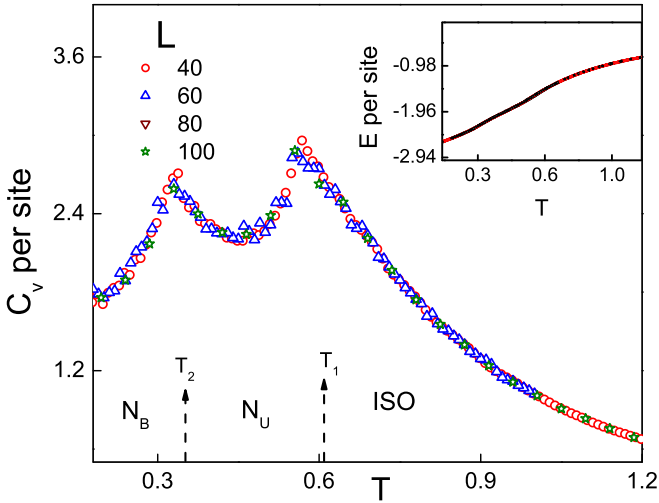


FIG. 1. Temperature variation of specific heat (per site) at lattice sizes  $L = 40, 60, 80, 100$ . Inset shows the temperature variation of size-independent energy per site for different  $L$ . The data for sizes  $L = 40, 60$  is from RW ensembles while data for  $L = 80, 100$  is from B ensembles.

shows two cusps at temperatures  $T_1$  and  $T_2$ , indicating two phase transitions, and these are found to be independent of size. The inset shows the size independence of the energy per site. In a normal disordering transition, the specific-heat peak is a measure of the energy fluctuations and the (per site) peak scales with the system size. The size independence of the peak heights as well as of the profiles of their cusps are early pointers to a nonconventional, and possibly topological, origin for the occurrence of the transition [18,36]. Our results on the Binder's energy cumulant [35] at size  $L = 100$  (not shown here) indicate that both transitions appear continuous. We note that a continuous transition is to be expected, for example, if it has an underlying topological mechanism [37].

While discussing the other observables, we note that the site symmetry of this chosen model (with identical arms)  $C_{2v}$ , though distinct from other more commonly adopted site symmetries (like  $D_2$  or  $D_{2h}$ ), is not distinguishable as far as second rank tensor properties of the system are concerned (like orientational orders, for example) [38,39]. The characteristic properties, which are associated with the stable topological defects, are consequences of the symmetry ( $D_{2h}$ ) of the  $\mathcal{R}$  space (phase) symmetry only specified by the first fundamental group of the medium, and the site and phase symmetries that qualitatively differ. In the present model, for example,  $C_{2v}$  is Abelian without inversion symmetry, whereas the phase symmetry  $D_{2h}$  is non-Abelian and includes inversion. The topological variables observed are commensurate with the phase symmetry of the medium, which in turn flows from the symmetry of the terms in the Hamiltonian. The biquadratic interactions thus do not leave any room for the specific site-symmetry  $C_{2v}$  of this model to impact the observable topological observables.

Figure 2 shows the temperature variation of the uniaxial order parameter  $R_{00}^2$  and the biaxial order parameter  $R_{22}^2$  for different system sizes. At a given size, the sharp increase of uniaxial order near the high-temperature transition followed by a similar increase in the biaxial order at a lower temper-

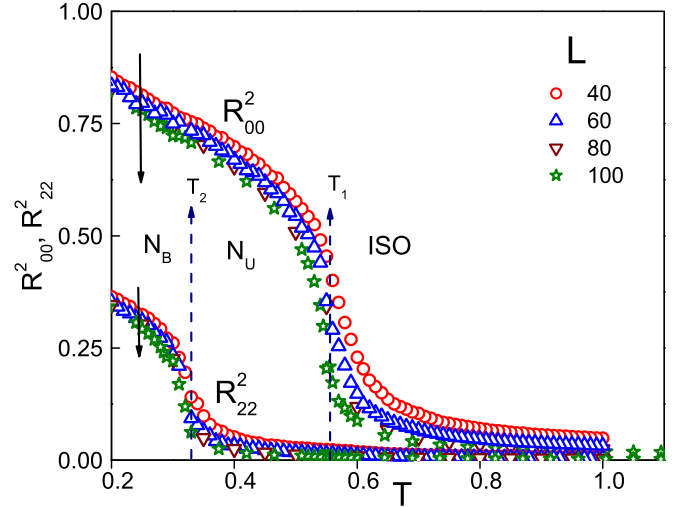


FIG. 2. Temperature variation of orientational order parameters at lattice sizes  $L = 40, 60, 80, 100$ . The data for sizes  $L = 40, 60$  is from RW ensembles while data for  $L = 80, 100$  is from B ensembles. (The arrows indicate increase in the size of the system).

ature signals changes of symmetry of the medium to a LC phase of uniaxial symmetry followed by biaxial symmetry. It is seen that the onset temperatures of both  $R_{00}^2$  and  $R_{22}^2$  shift to lower temperatures and their magnitudes decrease as the system size increases. The decrease of low-temperature orientational order with size is also not in line with the expected size dependence in conventional order-disorder transitions. Such unusual variations of order parameter are known to point typically to the topological character of the two transitions [40]. They betray the lack of long-range order in the low-temperature orientationally ordered phases due to the continuing presence of topological defects. Under the circumstances, these media do not strictly correspond to the conventional uniaxial and biaxial nematic phases owing to their qualitatively differing underlying microstructures. However, for convenience during discussion, they will continue to be still referred to, with this caveat in place.

The topological parameters (unbound defect density and topological order) provide direct evidence to infer about the transition more quantitatively. They show sharp changes at the onset of transition, clarifying the role of distinct classes of defects that the medium hosts. The temperature variation of the topological densities ( $d_x, d_y, d_z$ ) of the directors corresponding to  $(x, y, z)$  axes at different lattice sizes ( $L = 40, 60, 80, 100$ ) is depicted in Fig. 3. These are found to be size independent over the temperature range, but for small neighborhood regions near the two transitions. As the temperature is increased,  $d_x$  and  $d_y$  increase sharply near the lower temperature transition, whereas such an increase in  $d_z$  is in the vicinity of the higher temperature transition. Their minor size dependencies near the two transition regions are magnified in the insets for lattice sizes  $L = 40, 100$ . These size dependencies of the defect densities are reflective of the effect of the system size on the process of onset of the BKT-type mechanism of the respective transitions.

Figure 4 shows the  $C_v$  plotted along with derivatives of the topological densities ( $\Delta d_\alpha, \alpha = x, y, z$ ) as a function of

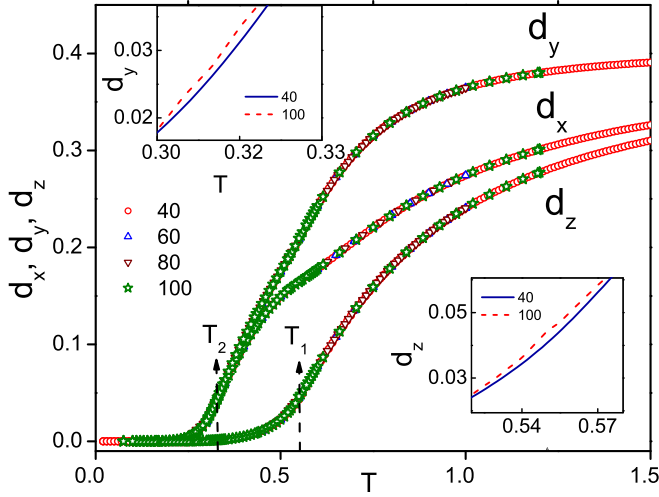


FIG. 3. Temperature variation of topological densities  $d_x, d_y, d_z$  at lattice sizes  $L = 40, 60, 80, 100$ . The insets show the slight size dependence for sizes  $L = 40, 100$  in (a) the biaxial phase near  $T_2$  for  $d_y$  and (b) the uniaxial phase near  $T_1$  for  $d_z$ .

temperature. The cusps of  $\Delta d_\alpha$  ( $\alpha = x, y, z$ ) associated with the major and minor axes bear striking correlation with those of the specific heat, near the transitions from the disordered phase initially to the uniaxial, and followed by biaxial phases, respectively. The derivative cusps are indicative of the rate of progression of the proliferation of the unbound defects immediately after the onset of the unbinding mechanism of the respective transitions. They drive the sharp changes in the specific heat variation, indicating absorption of energy due to the unbinding process [4,5,18,33,41]. The two cusps are separated in temperature (by  $\sim 0.16$ ) which is large enough to distinguish the two transitions, but not sufficient to decouple and provide data on  $G(r, T)$  which is free from pre-translational effects. Starting from the low temperature end, we note that the temperature variations of  $\Delta d_x$  and  $\Delta d_y$  are practically coincident at the onset of the lower transition at  $T_2$ . They tend

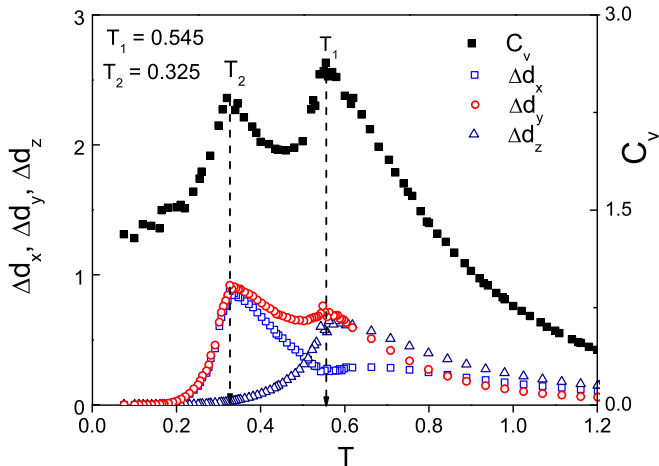


FIG. 4. Temperature variation of the specific heat  $C_v$  superposed on the temperature derivatives of topological densities ( $\Delta d_x, \Delta d_y, \Delta d_z$ ) at lattice size  $L = 100$ .

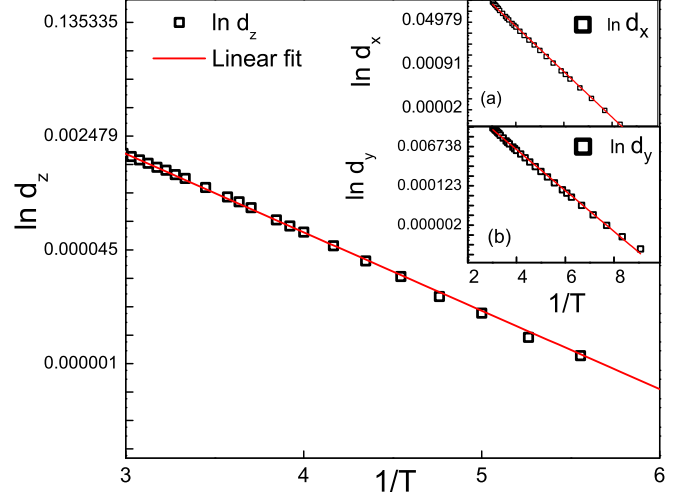


FIG. 5. Plot of natural logarithm of defect density  $d_z$  versus the inverse temperature at lattice size  $L = 100$ . A straight line fit to the curve gives an estimate of activation energy for  $z$  defects. Insets show similar plots for (a)  $d_x$  and (b)  $d_y$ .

to differ significantly with the onset of the high temperature transition (in the vicinity of  $T_1$ ), i.e., at the onset of the proliferation of the major axis defects. In the disordered state,  $\Delta d_x$  and  $\Delta d_z$  converge in the high temperature limit, and their limiting values are smaller than the saturation value of  $\Delta d_y$ . These densities are measures of mean distances between the corresponding unbound defects, and determine relative characteristic lengths associated with spatial variations of the corresponding orientational correlations [18].

Focusing on the differing profiles of the production rate of unbound defects (Fig. 4) of the minor axes above  $T_2$ , the rate of proliferation of the  $y$ -axis defects appears to be only marginally affected from its decay profile (with a small cusp at  $T_1$ ) and is otherwise a continuation of its prior path. The growth of the unbound defects of the molecular  $x$  axis, on the other hand, are more profoundly influenced at  $T_1$ . The rapid decay of the proliferation rate is temporarily arrested near  $T_1$  before starting to decrease, but at much slower rate. Interestingly, above  $T_1$  the rates of saturation of the  $z$ -axis and  $x$ -axis defect densities seem to be coincident asymptotically in the high-temperature limit. These subtle qualitative differences in  $\Delta d_x$  and  $\Delta d_y$  variations near  $T_1$  are indicative of the coupling between the uniaxial and biaxial molecular tensors of the interacting sites (i.e.,  $\gamma \neq 0$ ). For a Hamiltonian with  $\gamma = 0$ , for example, the Hamiltonian treats both the minor axes on equal footing and their  $\Delta d_x$  and  $\Delta d_y$  profiles were found identical at the two transitions through the entire temperature range. The defect densities are thus very subtle but definitive indicators of the nature of the tensor-coupling interactions in the Hamiltonian.

The onset of the topological transition is initiated by a thermal activation process and we estimate this energy for each category of defects by fitting their data on initial growth of the unbound defect density to the Arrhenius equation [33]. Figure 5 depicts variation of the three defect densities (on a log scale) with respect to the inverse of temperature. The data fit very satisfactorily to straight lines in each case, and the

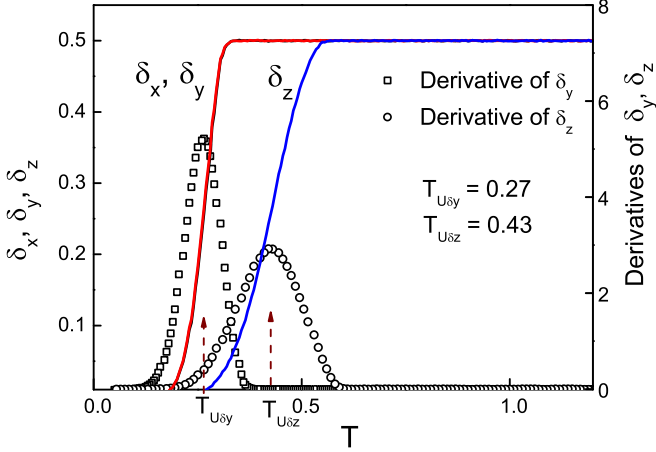


FIG. 6. Temperature variation of topological order parameters  $\delta_x, \delta_y, \delta_z$  at  $L = 100$ . The dotted curves are the temperature derivatives of  $\delta_z$  and  $\delta_y$  having peaks at  $T_{U\delta_z}$  and  $T_{U\delta_y}$ .

magnitudes of the slopes are measures of the activation energies associated with the unbinding mechanisms of the respective transitions. This energy value for the transition at  $T_1$  due to  $z$ -axes defects is  $E_{0z} = 2.75 \pm 0.023$  (Fig. 5). The unbound defects of  $x$  and  $y$  axes are activated with identical energy and the corresponding values are :  $E_{0x} = E_{0y} = 2.08 \pm 0.017$  (insets of Fig. 5).

Figure 6 depicts the temperature variation of the topological variables of the  $(x, y, z)$  axes ( $\delta_x, \delta_y, \delta_z$ ) related to the corresponding topological orders and their temperature derivatives, at  $L = 100$ . As the system is cooled starting from the isotropic phase,  $\delta_z$  sharply decreases from a constant value of 0.5 at the onset of the high-temperature transition, and in the completely (topologically) ordered state (of  $z$ -axes defects), its value is zero. We note that the corresponding parameters of  $x$  and  $y$  axes ( $\delta_x, \delta_y$ ) are unaffected by this transition. They show, however, similar changes with temperature at the second transition. These sharp changes in  $\delta$  variables are definitive markers identifying the category of defects associated with the particular transition. The inflexion point of their decay is the transition temperature where the unbinding mechanism is formally initiated. We calculated the corresponding transition temperatures for this system size ( $L = 100$ ) as  $T_{U\delta_z}(L) = 0.43 (\pm 0.005)$  and  $T_{U\delta_x}(L) = T_{U\delta_y}(L) = 0.27 (\pm 0.005)$ , as indicated in Fig. 6. The size dependence of the topological order profiles is shown in Fig. 7. The lowering of transition temperatures with increase in size is in accord with similar size variation of the onset of orientational order parameters (Fig. 2).

Correlation functions  $G(r, T)$  of the  $(X, Y, Z)$  directors at  $L = 100$  at certain chosen temperatures (out of the data collected at 60 temperatures) are shown in Fig. 8, covering all three phases of the model. These follow specific analytically expressible decays in the isotropic (above  $T_1$ ) and biaxially symmetric (below  $T_2$ ) phases. These fit very well to exponential decays with a different  $T$ -dependent correlation lengths for each director, as  $G(r, T) = A \exp(-r/\xi_\alpha(T)) + C$ , ( $\alpha = x, y, z$ ) in the isotropic phase. In the biaxial phase, they follow power-law decays, each with its own

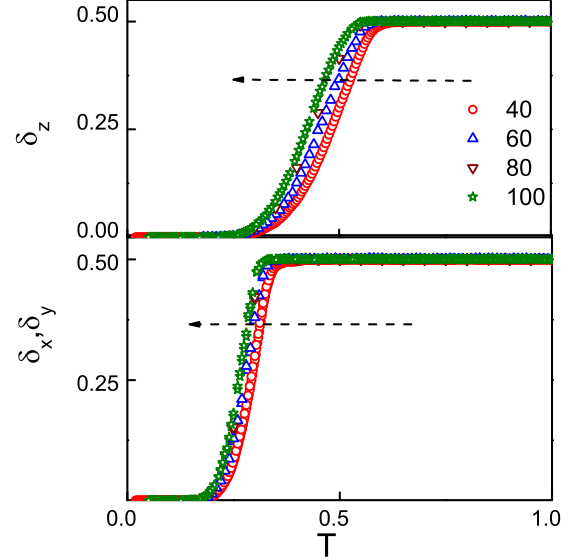


FIG. 7. Temperature variation of topological order parameters  $\delta_x, \delta_y, \delta_z$  at lattice sizes  $L = 40, 60, 80, 100$  (the arrows indicate the increase in system size).

$T$ -dependent exponent, as  $G(r, T) \approx r^{-\eta_\alpha(T)}$ , ( $\alpha = x, y, z$ ). For temperatures in the range  $0.3 \leq T \leq 0.555$  (uniaxial symmetry), correlation functions of  $X$  and  $Y$  directors do not fit satisfactorily to either a power law or an exponential decay, whereas the correlation function of the  $Z$  director fits very well to a power law.

The temperature variation of the power law exponents in the uniaxial and biaxial phases is depicted in Fig. 9.  $\eta_x(T)$  and  $\eta_y(T)$  [Fig. 9(a)] decrease linearly with temperature as  $T \rightarrow 0$  in the biaxial phase with different slopes. They are expected to vanish at  $T = 0$  in large enough samples approximating the thermodynamic result. In the present case ( $L = 100$ ), they tend to a nonvanishing value in this temperature limit, which is an artifact of the finite size of the system. We note that  $\eta_x(T) = 0.26$  and  $\eta_y(T) = 0.31$  at the unbinding temperatures  $T_{U\delta_x} = T_{U\delta_y} = 0.27$ , reasonably close to the mean-field expected value of 0.25 (for 2D-XY and planar LL model [40]). Figure 9(b) depicts variations of  $\eta_z(T)$  over the temperature range covering uniaxial and biaxial symmetric phases, with a value  $\eta_z = 0.25$  at  $T_{U\delta_z} = 0.43$ .

Temperature dependencies of the three correlation lengths in the isotropic phase,  $\xi_x(T)$ ,  $\xi_y(T)$ , and  $\xi_z(T)$ , are depicted in Fig. 10. We observe the anticipated correspondence of the magnitudes of the unbound defect densities associated with the three directors above the high-temperature transition (Fig. 3), with their respective correlation lengths. The  $y$ -axis defects have a lower correlation length  $\xi_y(T)$  value (until their divergences set in) than the others. The  $x$ - and  $z$ -director defects have comparable values, with  $\xi_z(T)$  marginally becoming greater than  $\xi_x(T)$  particularly as the transition point is reached from above. This is also in accord with the observations from their defect densities, and establishes clearly the origin of length scales in this phase.

For the transition observed at  $T_1$ , the critical behavior of  $\xi_z(T)$  alone is obviously relevant. The differing divergences of the other two correlation lengths are reflective of the

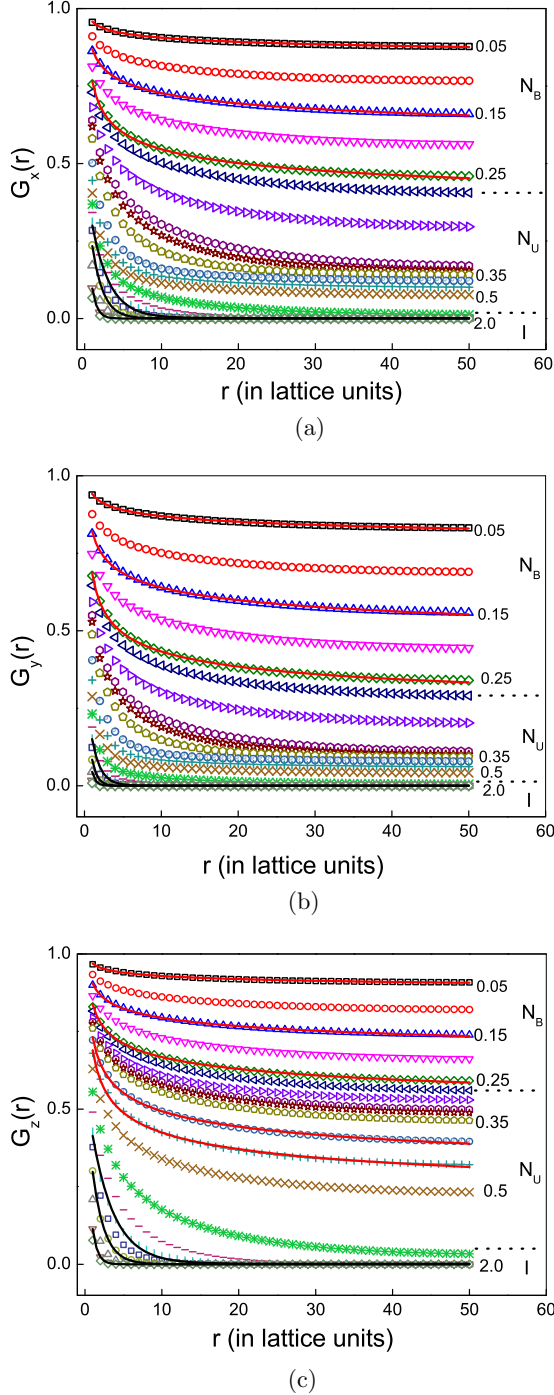


FIG. 8. Spatial variation of the correlation functions  $G(r)$  of the  $x$ ,  $y$ ,  $z$  directors ( $L = 100$ ) at chosen temperatures in the isotropic, uniaxial, and biaxial phases.  $G(r)$  fits to exponential decays in the isotropic phase (black solid line fit superposed on the data), power law decays (red dotted line fit superposed on the data) in the biaxial phase for all axes, whereas in the uniaxial phase only  $G_z(r)$  exhibits power law decay.

differential perturbations that the corresponding unbound defect densities suffer due to this transition. These indicate in part the manifestation of cross coupling of the uniaxial and biaxial tensors, in terms of a phenomenological description. The relevant correlation length  $\xi_z(T)$  should show essen-

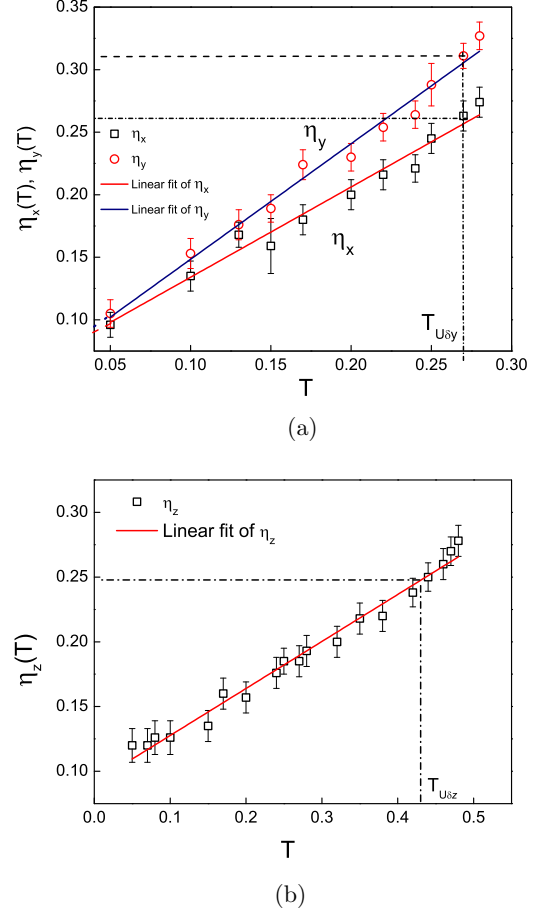


FIG. 9. Temperature variation of the power-law exponents (a)  $\eta_x(T)$ ,  $\eta_y(T)$  in the biaxial phase and (b)  $\eta_z(T)$  in uniaxial and biaxial phases.

tial divergence near a topological transition, unlike a simple divergence as in conventional transitions. The mean-field expression describing this near a topological transition arising from the sharp disappearance of the unbound defects is given by  $\xi(T) \approx \exp \left[ \frac{D}{(T-T_{U\delta})^\nu} \right]$  [5,15,16,42,43], where  $T_{U\delta}$  is the

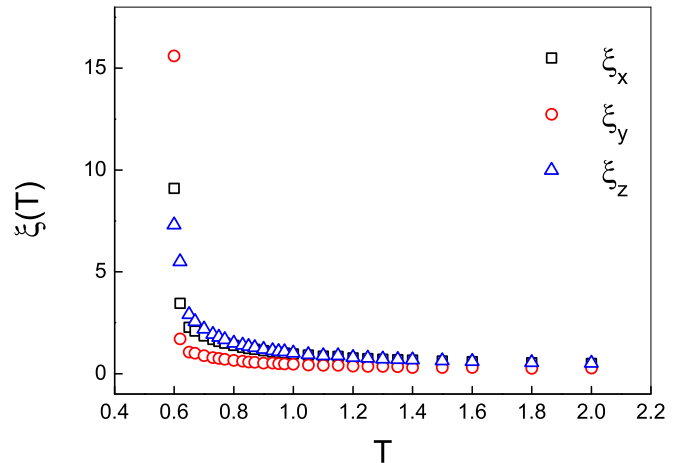


FIG. 10. Temperature variation of the correlation lengths  $\xi_x(T)$ ,  $\xi_y(T)$ , and  $\xi_z(T)$  of  $x$ ,  $y$ , and  $z$  defects at lattice size  $L = 100$ .



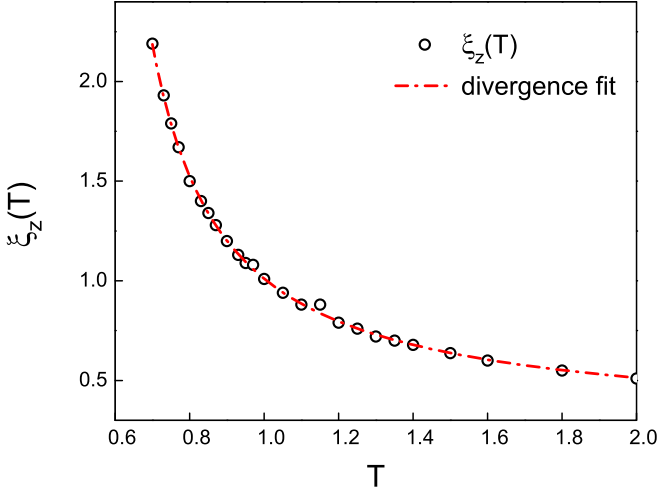


FIG. 11. Temperature variation of the correlation length  $\xi_z(T)$  of  $z$  defects at lattice size  $L = 100$ . The dash-dotted line is the divergence fit of  $\xi_z(T)$  as indicated in the text.

unbinding temperature determined earlier and  $\nu$  is the associated critical index. The fit using the predetermined value  $T_{U\delta z} = 0.43$ , shown in Fig. 11, yields  $\nu = 0.5 (\pm 0.025)$ , which compares very well with the mean-field value. The close proximity of the two transitions, together with the clear evidence of cross coupling interaction, prohibits single length scales for correlation functions associated with the minor axes in the uniaxial medium as was noted earlier, and hence no useful information could be inferred about the critical properties of the second transition.

Based on the known symmetry and the interarm angle of this model, we identify the corresponding representative point in the parameter space  $\Omega = (\xi, \gamma, \lambda)$  of the phenomenological model. Conventionally, the energy scale in these models is specified in units of  $\xi$ , which sets the degree of dominant coupling interaction among the uniaxial tensors of the interacting molecules. The choice of identical arms in the current model along with identical interaction strengths, reduces the space in the remaining  $(\gamma, \lambda)$  plane to a  $\theta$ -dependent trajectory, making this system a single parameter model, say  $\gamma(\theta)$ . It was shown in an earlier analysis [44] that the analytical expression of its Hamiltonian is identical with the well-investigated *dispersion model* [45,46]. Equation (1) then is recast in terms of phenomenological parameters as [44]

$$H \approx \{-G_{33} + 2\gamma(\theta)(G_{22} - G_{11}) - \gamma(\theta)^2 \times [2(G_{11} + G_{22}) - G_{33}]\}. \quad (2)$$

Here,  $\gamma(\theta) = (\cos^2 \theta/2 - \sin^2 \theta/2) = \cos \theta$ . Further,  $G_{ij} = P_2(f_{ij})$ ,  $P_2(\cdot)$  denotes the second Legendre polynomial and  $f_{ij} = (\mathbf{u}_i, \mathbf{v}_j)$  is the inner product. The sets of vectors  $(\mathbf{u}_i, i = 1, 2, 3)$  and  $(\mathbf{v}_j, j = 1, 2, 3)$  are the two orthonormal triads associated with molecules on the neighboring interacting sites. We note that in the absence of biaxial perturbation ( $\gamma(\theta) = 0$ , or  $\theta = 90^\circ$ ), the system condenses into a uniaxial nematic phase only, with the primary director

being determined by the average direction of the major axes, indexed as 3 ( $\mathbf{m}$  in phenomenological notation). In the present molecular model at that angle, the uniaxial nematic director points along the  $x$  axis of the molecular orthogonal triad, since the two orthogonal segments of the molecule are contained by construction in its  $yz$  plane. The identification of the remaining phenomenological axes  $\mathbf{e}$  and  $\mathbf{e}_\perp$  (indexed as 1 and 2) with the molecular  $y$  and  $z$  axes is not unique and depends on the sign of the model parameter  $\gamma(\theta)$ . As per the convention implied in Eq. (2),  $\mathbf{e}$  and  $\mathbf{e}_\perp$  are identified, respectively, with  $y$  and  $z$ . Thus this microscopic model is mapped in  $\Omega$  as a point (accurate to within four decimal places) with  $(\xi, \gamma, \lambda) = (1, -0.3746, 0.1403)$ , which is close to the corresponding Landau point  $(1, -0.3333, 0.1111)$  [14].

#### IV. CONCLUSIONS

This MC study reports the occurrence of two thermally driven topological transitions from a disordered phase of an ensemble of simple V-shaped molecules (bent at  $\theta = 112^\circ$ ) with a simple biquadratic Hamiltonian. The first transition leads to a topologically ordered phase involving the primary director and imparting uniaxial symmetry to the medium, and the second low-temperature one results in a fully (topologically) ordered LC medium with biaxial symmetry. Temperature variation data on the specific heat and orientational orders are consistent with the size dependencies expected in the case of topological transitions. Sharp variations in the topological parameters  $d_k$  and  $\delta_k$  corroborate these conclusions, besides determining the transition temperatures accurately. The self-similar structures seen in the low-temperature phase indicate complete topological ordering of the medium. The temperature data on densities of the unbound defects associated with different directors, besides providing quantitative information about the activation energies needed for unbinding processes, also betray differential coupling-interactions of minor axes with the major axis. In its phenomenological formulation, this observation corresponds to the presence of a cross-coupling term with significant  $\gamma$  value. Based on an established procedure for simple V-shaped models, the molecular-level interaction [Eq. (1)] is identified with the general biquadratic phenomenological Hamiltonian [Eq. (2)], with a single tunable  $\theta$ -dependent model parameter.

#### ACKNOWLEDGMENTS

We acknowledge the computational support from the Centre for Modelling Simulation and Design (CMSD) and the School of Computer and Information Sciences (DST PURSE-II Grant) at the University of Hyderabad. B.K.L. acknowledges financial support from Department of Science and Technology, Government of India vide Grant Ref. No. SR/WOS-A/PM-2/2016 (WSS) to carry out this work. S.D. acknowledges a grant from SERB (Ref. No. CRG/2019/000425). We wish to record our appreciation of the very meticulous perusal of the paper by the referees and thank them for their useful suggestions.

- [1] Y. Shen and I. Dierking, *Appl. Sci.* **9**, 2512 (2019).
- [2] J. Gong and L. Wan, *J. Phys. Chem. B*, **109**, 18733 (2005).
- [3] N. D. Mermin, *Rev. Mod. Phys.* **51**, 591 (1979).
- [4] V. L. Berezinskii, *Sov. Phys. JETP* **32**, 493 (1971); **34**, 610 (1972).
- [5] J. M. Kosterlitz and D. J. Thouless, *J. Phys. C* **6**, 1181 (1973).
- [6] P. Straley, *Phys. Rev. A* **4**, 675 (1971).
- [7] P. A. Lebowitz and G. Lasher, *Phys. Rev. A* **6**, 426 (1973).
- [8] D. Frenkel and R. Eppenga, *Phys. Rev. A* **31**, 1776 (1985).
- [9] R. L. Vink, *Eur. Phys. J. B* **72**, 225 (2009).
- [10] M. A. Bates and D. Frenkel, *J. Chem. Phys.* **112**, 10034 (2000).
- [11] R. Tavarone, P. Charbonneau, and H. Stark, *J. Chem. Phys.* **143**, 114505 (2015).
- [12] A. M. Sonnet, E. G. Virga, and G. E. Durand, *Phys. Rev. E* **67**, 061701 (2003).
- [13] S. Romano, *Physica A* **337**, 505 (2004).
- [14] F. Bisi, E. G. Virga, E. C. Gartland Jr., G. DeMatteis, A. M. Sonnet, and G. E. Durand, *Phys. Rev. E* **73**, 051709 (2006).
- [15] B. K. Latha and V. S. S. Sastry, *Phys. Rev. E*, **102**, 040701(R) (2020).
- [16] B. K. Latha and V. S. S. Sastry, *Phys. Rev. Lett.* **121**, 217801 (2018).
- [17] B. Kamala Latha and V. S. S. Sastry, *Liq. Cryst.* **45**, 2197 (2018).
- [18] H. Kunz and G. Zumbach, *Phys. Rev. B* **46**, 662 (1992).
- [19] S. Shabnam, S. D. Gupta, and S. K. Roy, *Phys. Lett. A* **380**, 667 (2016).
- [20] M. A. Bates and G. R. Luckhurst, *Phys. Rev. E* **72**, 051702 (2005).
- [21] N. Metropolis, A. W. Rosenbluth, M. N. Rosenbluth, A. H. Teller, and E. Teller, *J. Chem. Phys.* **21**, 1087 (1953).
- [22] F. Wang and D. P. Landau, *Phys. Rev. Lett.* **86**, 2050 (2001); *Phys. Rev. E* **64**, 056101 (2001).
- [23] K. Langfeld, B. Lucini, A. Rago, R. Pellegrini, and L. Bongiovanni, *J. Phys.: Conf. Ser.* **631**, 012063 (2015).
- [24] G. Brown, A. Rusanu, M. Daene, D. M. Nicholson, M. Eisenbach, and J. Fiddler, *J. Appl. Phys.* **109**, 07E161 (2011).
- [25] G. Shi, T. Wust, and D. P. Landau, *Phys. Rev. E* **94**, 050402(R) (2016).
- [26] C. H. Chan, G. Brown, and P. A. Rikvold, *Phys. Rev. E* **95**, 053302 (2017).
- [27] T. Vogel, Y. W. Li, and D. P. Landau, *J. Phys.: Conf. Ser.* **1012**, 012003 (2018).
- [28] D. Jayasri, V. S. S. Sastry, and K. P. N. Murthy, *Phys. Rev. E* **72**, 036702 (2005).
- [29] C. Zhou, T. C. Schulthess, S. Torbrugge, and D. P. Landau, *Phys. Rev. Lett.* **96**, 120201 (2006).
- [30] B. Kamala Latha, R. Jose, K. P. N. Murthy, and V. S. S. Sastry, *Phys. Rev. E* **92**, 012505 (2015).
- [31] R. H. Swendsen and J. S. Wang, *Phys. Rev. Lett.* **58**, 86 (1987).
- [32] B. A. Berg, *Comput. Phys. Commun.* **153**, 397 (2003).
- [33] M. H. Lau and C. Dasgupta, *Phys. Rev. B* **39**, 7212 (1989).
- [34] B. Kamala Latha, G. Sai Preeti, K. P. N. Murthy and V. S. S. Sastry, *Comput. Mater. Sci.* **118**, 224 (2016).
- [35] K. Binder, *Phys. Rev. Lett.* **47**, 693 (1981); *Z. Phys. B: Condens. Matter* **43**, 119 (1981).
- [36] C. Chiccoli, P. Pasini, and C. Zannoni, *Physica A* **148**, 298 (1988).
- [37] U. Gerber, W. Bietenholz, and F. G. Rejon-Barrar, *J. Phys.: Conf. Ser.* **651**, 012010 (2015).
- [38] S. Turzi and F. Bisi, *Nonlinearity* **30**, 4277 (2017).
- [39] S. Turzi and F. Bisi, *Mol. Cryst. Liq. Cryst.* **684**, 37 (2019).
- [40] A. I. Farinas-Sanchez, R. Botet, B. Berche, and R. Paredes, *Condens. Matter Phys.* **13**, 13601 (2010).
- [41] C. Holm and W. Janke, *J. Phys. A: Math. Gen.* **27**, 2553 (1994).
- [42] R. Kenna, *Condens. Matter Phys.* **9**, 283 (2006).
- [43] H. Kawamura, A. Yamamoto, and T. Okubo, *J. Phys. Soc. Jpn.* **79**, 023701 (2010).
- [44] S. Romano, *Physica A* **339**, 511 (2004).
- [45] F. Biscarini, C. Chiccoli, P. Pasini, F. Semeria, and C. Zannoni, *Phys. Rev. Lett.* **75**, 1803 (1995).
- [46] R. Berardi, L. Muccioli, S. Orlandi, M. Ricci, and C. Zannoni, *J. Phys.: Condens. Matter* **20**, 463101 (2008).